

ChemComm

Accepted Manuscript



This is an *Accepted Manuscript*, which has been through the Royal Society of Chemistry peer review process and has been accepted for publication.

Accepted Manuscripts are published online shortly after acceptance, before technical editing, formatting and proof reading. Using this free service, authors can make their results available to the community, in citable form, before we publish the edited article. We will replace this *Accepted Manuscript* with the edited and formatted *Advance Article* as soon as it is available.

You can find more information about *Accepted Manuscripts* in the [Information for Authors](#).

Please note that technical editing may introduce minor changes to the text and/or graphics, which may alter content. The journal's standard [Terms & Conditions](#) and the [Ethical guidelines](#) still apply. In no event shall the Royal Society of Chemistry be held responsible for any errors or omissions in this *Accepted Manuscript* or any consequences arising from the use of any information it contains.

Tubular perovskite solar cell: an improvement of charge separation at perovskite/HTM interface

Received 00th January 20xx,
Accepted 00th January 20xx

Xueping Zong,^{a,b} Zhe Sun,^{*a} Wang Hui,^a Jiang Wang,^a Mao Liang^a and Song Xue^{*a}

DOI: 10.1039/x0xx00000x

www.rsc.org/

Organolead iodide perovskite showing tubular morphology was fabricated onto mesoporous TiO₂ film via one-step spin-coating procedure. These perovskite tubes with the external diameter of 1 μm were found to facilitate the charge separation at perovskite/hole-transport material (HTM) interfaces. This engenders the tubular perovskite device showing a higher fill factor over the device with planar perovskite, and improves power conversion efficiency accordingly.

In the last two years, the advent of organometal halide perovskite solar cells (PeSCs) has drawn worldwide attention because of their low cost, easy-fabrication, and excellent power conversion efficiency reaching to 17.9%.¹ Since the seminal work by Kim et al.,² all-solid-state PeSC is typically fabricated as p-i-n architecture in which mesoporous or planar metal oxide layer, e.g. TiO₂, Al₂O₃ and ZnO, and hole transport layer (HTL) are employed for extracting photo-generated electrons and the separated holes, respectively.³ Between the two charge-collecting layers, methylammonium lead iodide CH₃NH₃PbI₃ layer with the thickness of several hundreds of nanometers is deposited, which serves as not only a light-harvesting component but a conductor for transporting a part of the separated excitons. Recent investigations have shown the vital importance of controlling the metal oxide/perovskite and perovskite/HTL interfaces for impeding the charge recombination. In this regard, diverse experimental protocols, including one or two-step deposition, vapor-assisted solution processing, and surface modification by amino acids, have been developed for tailoring the morphology of perovskite layer and improving its contact to metal oxide surfaces.⁴ CH₃NH₃PbI₃ crystal films appearing as nanorod clusters have been fabricated on the top surfaces of ZnO mesoporous layer as well as poly(3,4-ethylenedioxythiophene):

poly(styrene sulfonic acid) (PEDOT:PSS).⁵ It was showed that the presence of nanorods results in the pin-holes in perovskite film. As a consequence, light absorbance of the nanorods is inferior to that of planar film due to its incomplete surface coverage. Very recently, Im et al. have shown the advantages of non-planar perovskite nanowires in accelerating the rate of the charge separation at the perovskite/HTL interfaces.⁶ However, the length of the prepared nanowires is several ten microns. This probably affects the electron transport along the nanowires. In this paper, we report the fabrication of CH₃NH₃PbI₃ tubes with the diameter of several hundreds of nanometers and the height of several microns. These tubes growing above the mesoporous TiO₂ layer were shown to enhance electron lifetime by five times and hence improve cell parameters of the perovskite cells.

Tubular perovskite layer was attained by spin-coating CH₃NH₃PbI₃/dimethylformamide (DMF) solution with the concentration of 19 wt% onto mesoporous TiO₂ scaffold. For comparison, planar perovskite layer was also fabricated by 40 wt% perovskite precursor in which a mixture of γ-butyrolactone (GBL)

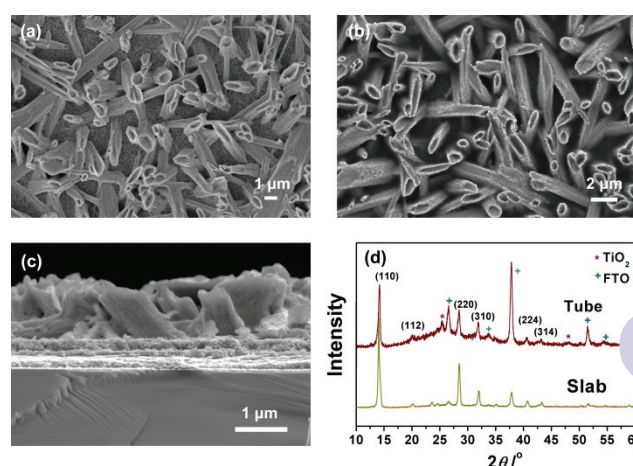


Fig. 1 Top view SEM images of (a) tubular perovskite layer and (b) spiro-OMeTAD soaked tubular perovskite layer. (c) Cross-sectional image of tubular perovskite/TiO₂/FTO film. (d) XRD patterns of perovskite tube and slab.

^aTianjin Key Laboratory of Organic Solar Cells and Photochemical Conversion, School of Chemistry & Chemical Engineering, Tianjin University of Technology, Tianjin 300384, P. R. China. E-mail: zhesun@tjut.edu.cn, xuesong@ustc.edu.cn; Fax: +86-22-60214252 Tel: +86-22-60214250

^bSchool of Materials Science and Engineering, Tianjin University of Technology, Tianjin 300384, P. R. China.

† Electronic Supplementary Information (ESI) available: Experimental details, additional morphologies of perovskite tube and slab, Nyquist plots of IMPS/IMVS, UV-Vis spectra. See DOI: 10.1039/b000000x/

COMMUNICATION

Journal Name

and dimethyl sulphoxide (DMSO) (7:3 v/v) was used as solvent. The cell fabrication details are described in the ESI.† Note that the solution recipes employed here were in line with the $\text{CH}_3\text{NH}_3\text{PbI}_3$ precursors in the preparation of quantum dot dye-sensitized solar cells.⁷ We found that the variation of solvent engenders a substantial change of perovskite morphology. As indicated in Fig. 1(a), the use of DMF results in the formation of perovskite tubes on the top surface of TiO_2 layer. And Fig. 1(b) shows that spiro-OMeTAD can be readily deposited into the perovskite forest, forming a continuous hole-transport phase. The cross-section of perovskite tubes shown in Fig. 1(c) illuminates the length of the tubes is about several microns, shorter than the reported nanowires by one order of magnitude.⁶ Thereby, a lower resistance of electron transport in our perovskite tubes is expected. Moreover, we found that these tubes are hexagonal rather than circle, and constructed of $\text{CH}_3\text{NH}_3\text{PbI}_3$ crystals with the size of 100 nm. These are shown in Fig. S1 a and b of the ESI.† By using the solvent of GBL/DMSO mixture, compact perovskite slab was fabricated (see Fig. S1(c)). XRD spectra (Fig. 1(d)) indicate that both perovskite tube and slab display the same space group of $I4/mcm$, implying tetragonal $\text{CH}_3\text{NH}_3\text{PbI}_3$ structure.^{6,8} Besides that, the tube shows a weaker (220) peak relative to the slab sample. This is in agreement with the result of perovskite nanowires, which is relative to their difference in mesoscopic morphology.⁶ The variation of $\text{CH}_3\text{NH}_3\text{PbI}_3$ morphology is probably dependent of precursor concentration and the rate of solvent evaporation. For the tubular sample, $\text{CH}_3\text{NH}_3\text{PbI}_3$ precursor concentration is about half of that for preparing the perovskite slab. And DMF is relatively volatile compared with the GBL/DMSO mixture. For these reasons, the evaporation of the $\text{CH}_3\text{NH}_3\text{PbI}_3$ /DMF precursor brings forth to lower nucleation density and larger critical nucleus radius.⁹ As a consequence, $\text{CH}_3\text{NH}_3\text{PbI}_3$ crystals tend to assemble into mesoscopic tubes for decreasing Gibbs free energy. For the GBL/DMSO based precursor, higher $\text{CH}_3\text{NH}_3\text{PbI}_3$ concentration leads to larger nucleation density, and helps to form planar layer.

To elucidate the effects of perovskite morphology on charge separation characteristics, we determined IMPS and IMVS response curves for both tubular and planar $\text{CH}_3\text{NH}_3\text{PbI}_3$ based PeSCs. Typical curves are displayed in Fig. S2 of the ESI.† Time constants of electron transport (τ_{tr}) and recombination (τ_n) were obtained from the characteristic frequency at the minimum imaginary component of IMPS and IMVS, respectively.¹⁰ As depicted in Fig. 2 (a), recombination time constant τ_n for perovskite tube based devices is higher than that of the planar ones by about 2-4 fold. Accordingly, tubular PeSCs show a higher electron density. This result reflects the decreased recombination rate by using tubular perovskite component. It is known that the conductivity of $\text{CH}_3\text{NH}_3\text{PbI}_3$ renders the recombination of PeSCs occurring at perovskite/HTL and TiO_2 /perovskite interfaces simultaneously.^{3,11} Therefore, the retarded recombination could be attributed to the tubular perovskite frame because the tube forest brings out larger surface for the interfacial charge separation with spiro-OMeTAD phase. In contrast to the decreased recombination rate, electron transport time for tubular PeSCs, as Fig.2 (b) indicated, is nearly equivalent to that of the planar devices. It means that tubular morphology has no apparent influence on the charge carrier transport in $\text{CH}_3\text{NH}_3\text{PbI}_3$ phase. This is consistent to the fact that perovskite tubes have the crystalline structure similar to the planar ones. Besides this, the length of the

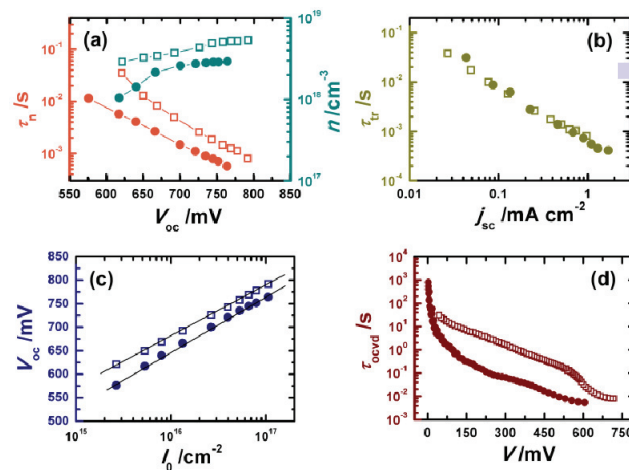


Fig. 2 (a) Plots of recombination time constant and electron density versus open circuit voltage. (b) Plot of electron transport time constant versus short circuit current density. (c) Plot of open circuit voltage versus photon flux. Solid lines indicate the best fits with eq 1. (d) Plot of open circuit voltage decay. Hollow square and solid circle mark the devices based on tubular and planar perovskite, respectively.

tubes, as mentioned above, is ~ 1 μm , much shorter than the nanowires. Moreover, the plots of open circuit voltage (V_{oc}) against photon flux (I_0) for tubular and planar PeSCs display a semi-logarithm relation. From these curves, ideality factor (m) can be estimated by using the following expression,¹²

$$V_{oc} \propto \frac{mk_B T}{q} \ln I_0 \quad (1)$$

where q is the elementary charge, k_B is the Boltzmann constant, and T is the absolute temperature. It is found that ideality factors for tubular and planar PeSCs are 1.87 and 1.95, respectively. These values are roughly equal since the $\text{CH}_3\text{NH}_3\text{PbI}_3$ tubes and slab in this work are constituted of nearly identical perovskite nanocrystals, which bring forth to similar distribution of the surface states. Interestingly, the photoluminescence spectra of the two $\text{CH}_3\text{NH}_3\text{PbI}_3$ films almost coincide (see Fig. S4 of the ESI).† This further indicates the likeness of the surface state profiles of tubular and slab. Moreover, those ideality factors are also shown to deviate from unity, implying the importance of the recombination reaction via the surface states to energy loss. Additionally, sluggish recombination in tubular perovskite based devices was also illuminated by photovoltage decay technique.¹³ In Fig. 2(d), the evolution of electron lifetime in the dark (τ_{ocvd} , proportional, reversely to charge recombination rate) indicates perovskite tubes not only serve as light-collectors but also play a role in slowing down the recombination rate by about 20-fold. This result further implies that the tubular perovskite frame primarily decreases the recombination of the holes in HTL with the electrons injected in TiO_2 matrix rather than those localized in $\text{CH}_3\text{NH}_3\text{PbI}_3$ layer. The reason is that perovskite tubes are expected to accelerate the rate of back reaction with the free electrons inside perovskite forest due to its larger surface area. Our observations, however, do not support this hypothesis. Furthermore, the primary pathway

charge as depicted in Fig. 3, could be the electrons in TiO₂ film diffuse across the perovskite tubes and reduce the holes subsequently (Path I). Direct recombination at TiO₂/HTL interfaces (Path II) is less important. This assumption is based upon that fact that CH₃NH₃PbI₃ is more conductive relative to spiro-OMeTAD by two orders.^{3a} Therefore, incomplete coverage of the tubes over the TiO₂ layer limits the back reaction of the electrons crossing the CH₃NH₃PbI₃ layer. By contrast, the TiO₂ layer in the planar devices is fully covered by the CH₃NH₃PbI₃ slab. The enlarged perovskite region implies a stronger recombination.

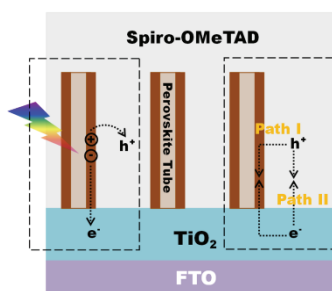


Fig. 3 Schematic of charge separation and recombination in tubular perovskite based devices. The recombination pathways across perovskite tube and TiO₂/spiro-OMeTAD interface are indicated as path I and path II, respectively.

The curves of incident power conversion efficiency (IPCE) for tubular and planar perovskite based devices are displayed in Fig. 4(a). We observed that planar perovskite cells yield an IPCE slightly over the tubular ones. This is consistent to the results of short circuit current density (J_{sc}) as indicated in Fig. 4(d). However, Fig. 4(b) shows that the planar cells show a higher light-harvesting efficiency (η_{LH}) in the wavelength range from 400 to 750 nm for more loading amount of CH₃NH₃PbI₃ in those cells. According to the data of IPCE and η_{LH} , we obtained charge collection efficiency (η_{COL}) by using the expression of $\eta_{COL} = IPCE/\eta_{LH}$.^{1b} And η_{COL} is plotted as a function of wavelength in Fig. 3(c). We can see the tubular cells yields a higher η_{COL} over the planar counterparts. It supports our conclusion that the usage of tubular perovskite frame leads to a limited interfacial recombination and more efficient charge collection in turn. Moreover, j - V characteristics of the tubular and planar cells are depicted in Fig. 4(d). The corresponding photovoltaic parameters are summarized in Table 1. We found that cell efficiency (PCE) of tubular cell reaches 7.4 %, which is 1.7 times higher than the planar ones. The improved PCE is partly relative to the V_{oc} of tubular cells, which is 42 mV higher than the planar ones. More importantly, fill factor is improved greatly by using tubular perovskite frame, and series resistance is reduced accordingly. Certainly, this is due to the tubular structure of CH₃NH₃PbI₃, which decreases the effective area of perovskite for charge recombination.

In summary, we have prepared organometal halide perovskite solar cells in which mesoscopic CH₃NH₃PbI₃ tubes, serving as light-absorbing layer, were deposited successfully onto the top surface of TiO₂ film. Compared with traditional planar perovskite layer, tube-like perovskite frame is shown to promote charge separation at CH₃NH₃PbI₃/HTL interfaces, but do not affect the rate of charge

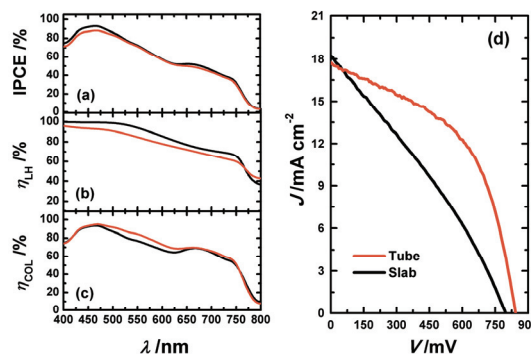


Fig. 4 Plots of (a) IPCE, (b) light harvesting efficiency, and (c) charge collection efficiency versus wavelength. (d) J - V characteristics for tubular and planar perovskite based devices.

Table 1 Photovoltaic parameters of the DSCs based on tubular and planar perovskite layers^a

PeSC	V_{oc} /mV	J_{sc} /mA cm ⁻²	FF	PCE /%	R_s / Ω cm ²	R_{sh} / Ω cm ²
Tube	841	17.6	0.50	7.4	9.67	154.2
Slab	799	18.3	0.30	4.3	25.3	47.4

^a All cells were irradiated under the illumination intensity of 100 mW cm⁻².

transport. Resultantly, tubular perovskite cells display higher open circuit voltage. However, this is not merely attributed to the enlarged contact area between CH₃NH₃PbI₃ and Spiro-OMeTAD. More importantly, perovskite tubes are found to decrease charge recombination rate. According to photovoltage decay measurements, tubular perovskite based devices display the recombination slower than the planar counterpart by 20-fold. The retarded recombination cannot be attributed to the variation of the surface states of CH₃NH₃PbI₃ nanocrystals. Instead, it is likely originated from the tube-like morphology. Certainly, the presence of CH₃NH₃PbI₃ tubes results in the loss of light-harvesting. However, the improved charge collecting efficiency offsets this energy loss and leads to a much higher fill factor. Thereby, the fabrication of perovskite tubes with larger loading density in the future work is expected to enhance spectral responses and maintain sluggish recombination simultaneously.

The support of the National Nature Science Foundation of China (21103123) and Tianjin Natural Science Foundation (13JCZDJC32400) is gratefully acknowledged.

Notes and references

- (a) A. Kojima, K. Teshima, Y. Shirai and T. Miyasaka, *J. Am. Chem. Soc.*, 2009, **131**, 6050–6051; (b) J. Burschka, N. Pellet, S. Moon, R. Humphry-Baker, P. Gao, M. K. Nazeeruddin and M. Grätzel, *Nature*, 2013, **499**, 316–319; (c) N. Park, *J. Phys. Chem. Lett.*, 2013, **4**, 2423–2429.
- H. S. Kim, C. R. Lee, J. H. Im, K. B. Lee, T. Moehl, A. Marchioni, S. J. Moon, R. Humphry-Baker, J. H. Yum, J. E. Moser, M. Grätzel and N. G. Park, *Sci. Rep.*, 2012, **2**, 591.
- (a) M. M. Lee, J. Teuscher, T. Miyasaka, T. N. Murakami and H. J. Snaith, *Science*, 2012, **338**, 643–647; (b) D. Liu and T. L. Kelly, *Nature Photonics*, 2014, **8**, 133–138; (c) J. Shi, Y. Luo, H. Wei, J. Luo, J. Dong, S. Lv, J. Xiao, Y. Xu, L. Zhu and X. Xu, *ACS Appl. Mater. Interfaces*, 2014, **6**, 9711–9718; (d) T. Leijtens, et al.

- D. Stranks, G. E. Eperon, R. Lindblad, E. M. Johansson, I. J. McPherson, H. Rensmo, J. M. Ball, M. M. Lee and H. J. Snaith, *ACS Nano*, 2014, **8**, 7147–7155.
- 4 (a) Y. Xu, L. Zhu, J. Shi, S. Lv, X. Xu, J. Xiao, J. Dong, H. Wu, Y. Luo and D. Li, *ACS Appl. Mater. Interfaces*, 2015, **7**, 242–2248; (b) M. Liu, M. B. Johnston and H. J. Snaith, *Nature*, 2013, **501**, 395–398; (c) L. Zuo, Z. Gu, T. Ye, W. Fu, G. Wu, H. Li and H. Chen, *J. Am. Chem. Soc.*, 2015, **137**, 2674–2679.
- 5 Y. Jeon, S. Lee, R. Kang, J. Kim, J. Yeo, S. Lee, S. Kim, J. Yun and D. Kim, *Scientific Reports*, 2014, **4**, 6953–1–4.
- 6 J.-H. Im, J. Luo, M. Franckevičius, N. Pellet, P. Gao, T. Moehl, S. M. Zakeeruddin, M. K. Nazeeruddin, M. Grätzel and N.-G. Park, *Nano Lett.*, 2015, **15**, 2120–2126.
- 7 J. H. Im, C. R. Lee, J. W. Lee, S. W. Park and N. G. Park, *Nanoscale*, 2011, **3**, 4088–4093.
- 8 D. H. Cao, C. C. Stoumpos, C. D. Malliakas, M. J. Katz, O. K. Farha, J. T. Hupp and M. G. Kanatzidis, *APL Mater.*, 2014, **2**, 091101–1–4.
- 9 (a) Y. Tidhar, E. Edri, H. Weissman, D. Zohar, G. Hodes, D. Cahen, B. Rybtchinski and S. Kirmayer, *J. Am. Chem. Soc.*, 2014, **136**, 13249–13256. (b) H. Gao, C. Bao, F. Li, T. Yu, J. Yang, W. Zhu, X. Zhou, G. Fu and Z. Zou, *ACS Appl. Mater. Inter.*, 2015, **7**, 9110–9117. (c) N. Yantara, F. Yanan, C. Shi, H. A. Dewi, P. P. Boix, S. G. Mhaisalkar and N. Mathews, *Chem Mater.*, 2015, **27**, 2309–2314.
- 10 (a) Y. Zhao and K. Zhu, *J. Phys. Chem. Lett.*, 2013, **4**, 2880–2884; (b) D. Bi, L. Yang, G. Boschloo, A. Hagfeldt and E. M. J. Johansson, *J. Phys. Chem. Lett.*, 2013, **4**, 1532–1536; (c) K. Zhu, N. R. Neale, A. Miedaner and A. J. Frank, *Nano Lett.*, 2007, **7**, 69–74.
- 11 H. J. Snaith, *J. Phys. Chem. Lett.*, 2013, **4**, 3623–3630.
- 12 (a) Z. Sun, R. Zhang, H. Xie, H. Wang, M. Liang and S. Xue, *J. Phys. Chem. C*, 2013, **117**, 4364–4373; (b) E. Guillén, L. M. Peter, and J. A. Anta, *J. Phys. Chem. C*, 2011, **115**, 22622–22632; (c) J. R. Jennings and Q. Wang, *J. Phys. Chem. C*, 2010, **114**, 1715–1724.
- 13 (a) P. R. F. Barnes, K. Miettunen, X. Li, A. Y. Anderson, T. Bessho, M. Grätzel and B. C. O'Regan, *Adv. Mater.*, 2013, **25**, 1881–1922. (b) J. Halme, P. Vahermaa, K. Miettunen and P. Lund, *Adv. Engery Mater.*, 2010, **22**, E210–E234.